

Computational Chemistry Modeling and Design of Photoswitchable Alignment Materials for Optically Addressable Liquid Crystal Devices

Introduction

Photoalignment technology has received great interest as an alternative to buffed alignment layers for generating high-quality, uniform molecular alignment in liquid crystal (LC) devices. Numerous examples exist in the literature where photoalignment technology has been applied to the development of new LC devices designed to solve difficult application problems in optics and photonics.^{1–9} The near-IR laser-damage resistance of coumarin-based photoalignment layers, developed at the Laboratory for Laser Energetics (LLE), approaches that of fused silica (over 60-J/cm², 1-ns pulse). In addition, these layers have made it possible to fabricate a wide variety of photoaligned LC devices for high-peak-power laser applications, including wave plates, beam shapers, apodizers, and radial polarization converters.^{1–4} Certain classes of photosensitive materials (e.g., azobenzenes and spiropyrans) can undergo *reversible* changes in molecular shape when exposed sequentially to UV or visible light. For azobenzene materials, this photomechanical isomerization between the rod-like *trans* state and the bent *cis* state occurs rapidly and reversibly over time scales of milliseconds at energy levels in the UV and visible regions of <250 mW/cm² [Fig. 143.29(a)].^{10,11} For example, azobenzene molecules attached as pendants to a polymer back-

bone through a flexible hydrocarbon spacer chain can function as a photoactive “command surface.” These pendants, when deposited on the inner surfaces of an LC device as an alignment coating, can be switched optically between two different alignment states using low-incident-energy polarized UV and visible light.^{11–13} This photoisomerization of the azobenzene pendants on the alignment coating redirects the orientation of the LC material in contact with the coating surface in response to the wavelength of the polarized “write” (UV) or “erase” (visible) incident light. Depending on the molecular geometry of the polymeric command surface, the resultant LC reorientation could be constrained to occur either out of plane (orthogonal) or in plane (azimuthal) of the substrate. A conceptual drawing of this behavior is shown in Fig. 143.29(b).

In previously reported work, we identified a series of commercially available azobenzene photoswitchable alignment materials with 1054-nm, 1-ns laser-damage thresholds ranging from 28 to 67 J/cm², which is comparable to reported values for coumarin photoalignment materials used in passive photoaligned LC devices intended for high-peak-power laser applications.^{6,14} Such optically switchable azobenzene command surfaces are being investigated actively for use in an “optically

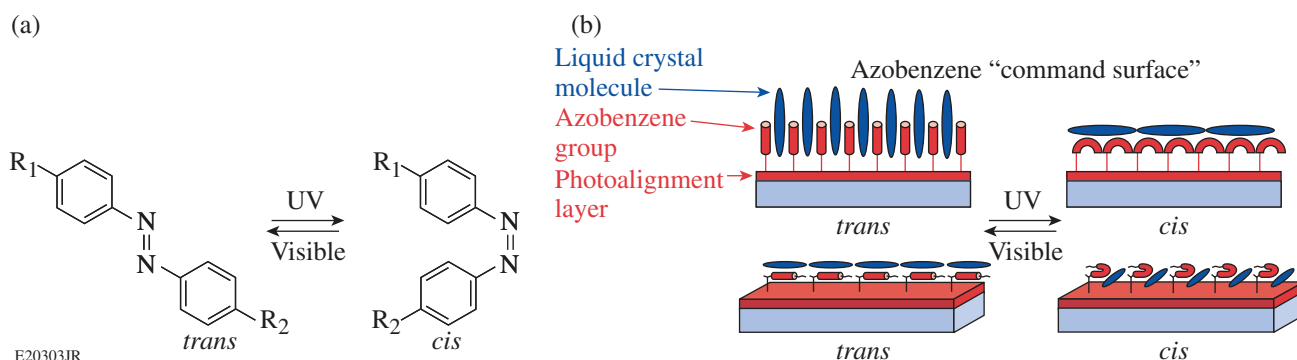


Figure 143.29

(a) *Trans*–*cis* isomerization in azobenzenes. (b) Photoswitchable “command surfaces” with azobenzene pendant groups. Azobenzene groups in the elongated *trans* state (left) cause liquid crystal (LC) molecules to adopt an orientation parallel to the azobenzene’s long molecular axis, while azobenzenes in the bent *cis* state (right) switch the orientation of the LC to a near-parallel orientation to the substrate to minimize their free energy. Depending on the molecular structure of the command surface, the resultant LC reorientation could be constrained to occur either out of the substrate plane (top) or in the plane of the substrate (bottom). This change in orientation induces a change in the polarization, phase, or amplitude of an incident optical beam.

addressed” LC spatial beam shaper concept intended for high-peak-power beam shaping in the 4-PW, 10-ps OMEGA EP Nd:glass solid-state laser at LLE.^{6,14} These optically addressed LC beam shapers are intended ultimately to replace electro-optical LC programmable spatial light modulators. Their application is limited to low-fluence locations in OMEGA EP beamlines because of the low laser-damage thresholds (250 to 500 mJ/cm² at 1054-nm, 1-ns pulse width) of the conductive oxide coatings required for their operation. A schematic diagram of the device concept is shown in Fig. 143.30. The LC molecules can be spatially varied between two alignment states by using low-energy polarized UV/visible light incident on the photoswitchable polymer alignment coating. This provides the in-system write/erase flexibility of electro-optical LC spatial beam shapers while eliminating conductive coatings and electrical interconnects that reduce laser-damage threshold and increase device fragility and complexity, respectively.

To date, the bulk of ongoing research in photoswitchable alignment coating technology is limited primarily to one class of photoactive chromophore (azobenzenes) in the form of low-molar-mass, water-soluble salts deposited either directly on the substrate surface or dispersed in a polymer binder. Progress in developing new photoalignment material systems with enhanced properties has been limited by the largely empirical “trial-and-error” approach, based on intuition and previous experience, that has been used to date. This process is time consuming, labor intensive, and wasteful of costly and potentially scarce materials resources because of the need to synthesize a large number of compounds to establish trends in physical properties. Applying computational chemistry methods to the design and development of new photoswitchable alignment materials

presents itself as an unprecedented opportunity to develop predictive capabilities that will lead to materials with low switching energies, enhanced bistability, and resistance to both write/erase fatigue and laser damage. The effectiveness of this approach has been demonstrated widely in the pharmaceutical industry and in the development of organic light-emitting diode materials and LC mesogens.¹⁵ As recently as 2015, computational studies of functional group effects on azobenzene chromophores are beginning to appear in the literature.^{16,17} Earlier studies to determine free-space volume,¹⁸ photoisomerization mechanisms, relationships between molecular structure and thermal relaxation,¹⁸ dipole moments, polarizabilities, Gibbs free energies, highest-occupied/lowest-unoccupied molecular orbital (HOMO/LUMO) band-gap energies, and chemical potentials using semiempirical computational chemistry methods have also been reported.¹⁷ In this work, we describe efforts to extend the application of the density functional theory (DFT) and time-dependent density functional theory (TDDFT) to determine the effect of molecular structure and functional groups on optical switching state energies in a series of novel photoswitchable alignment methacrylate and acrylamide polymers functionalized with azobenzene and spiropyran pendants.

Computational Chemistry Methods

Three types of computational methods are widely used in molecular mechanics and excited-state calculations. *Semiempirical* quantum chemical methods such as Zerner’s intermediate neglect of differential overlap (ZINDO)¹⁹ have the advantage of reduced computational time (and cost) by using existing experimental data with approximations to fit the calculations according to known parameters. This savings in computational time is obtained at a penalty; the method is

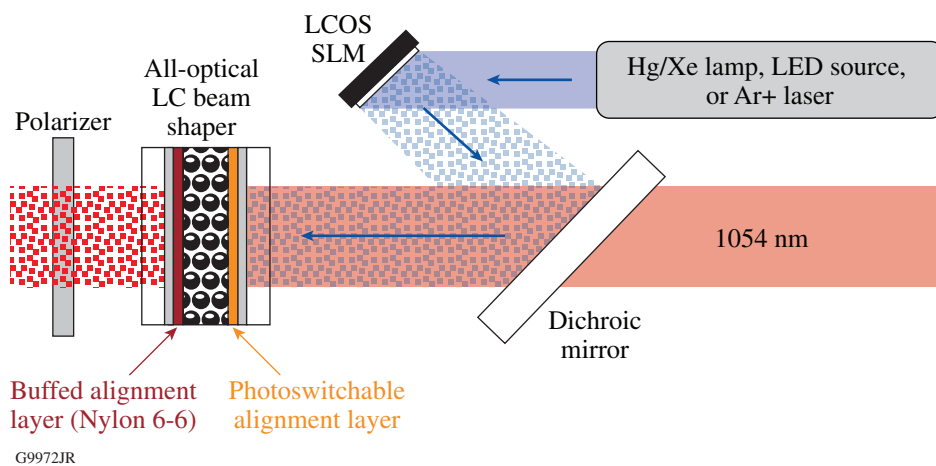


Figure 143.30

A conceptual layout for an all-optical beam shaper using a switchable photoalignment coating. Incident UV light from any number of incoherent or coherent sources [Hg/Xe lamp, light-emitting-diode (LED) source, or Ar+ or HeCd laser] provides the write illumination to a liquid crystal on silicon (LCOS) device, whose image plane is focused onto the photoalignment layer within the device. Patterns produced on the LCOS are written, erased, and rewritten on the photoalignment layer using either alternating UV incident polarizations or serial applications of UV and visible light. Alternatively, patterns can be written and erased directly using a raster-scanned polarized UV laser source. SLM: spatial light modulator.

limited in accuracy by the degree of similarity between the molecule being studied and existing molecules that are used as the parameter source. *Ab initio* methods are not based on existing experimental data but instead employ simulations that are run “from the beginning” using physical principles. The most frequently employed method for *ab initio* calculations is the Hartree–Fock method, which is based on several key assumptions: (1) all nuclei are motionless with respect to the electrons; (2) electron orbitals are expressed as one-electron functions centered on each atom; and (3) the multi-electron calculation of the model is given by the sum of all single-electron calculations of the molecule.²⁰ Relativistic effects and electron correlation effects (electron–electron interactions) are generally neglected. One disadvantage of the Hartree–Fock method is that its accuracy decreases with increasing molecular size.²⁰ Hartree–Fock calculations are usually used to approximate the ground-state energy of a molecular system. Post-Hartree–Fock methods such as the configuration interaction-single (CIS) method have been developed to allow excited-state calculations. Although these improved methods provide better accuracy, they do so at a substantially increased computational cost, are limited to single excitations, and are not highly accurate for larger molecules.^{20–22}

Recently, DFT and TDDFT have emerged as useful and efficient methods for calculating ground-state and excited-state properties, respectively.²³ These methods replace the many-electron wave function (a complex mathematical function in multidimensional space that takes into account individual electrons) used in Hartree–Fock calculations with an electron density function in three spatial dimensions. This approach greatly reduces the computational time without substantially sacrificing accuracy.²⁴ Figure 143.31 compares computed visualizations of wave functions versus electron density func-

tions for the same molecule. The TDDFT method models the evolution of the system’s electron density as a function of time in response to an external disturbance.²³ Jacquemin^{25,26} and Perpète²⁷ used TDDFT extensively to model the absorbance spectra of a series of indigo, nitro-diphenylamine, and anthraquinone-based organic dyes and consistently demonstrated the high accuracy of TDDFT for these materials. These results, along with our previous experience in using DFT and TDDFT for similar calculations in large, complex molecular systems,²⁸ led us to choose this computational method for our studies.

Computational Resources

All DFT and TDDFT calculations were conducted using one of two computer servers in the LLE Computing Facility (LCF): a Dell PowerEdge R710 server [8-core, 2.4-GHz Intel Xeon E5530 CPU (16 virtual cores with hyperthreading), 48 GB of memory connected to NFS4 computing storage over a 1-GB network] or an HP ProLiant SL250s Gen 8 server (24-core, 2.4-GHz Intel Xeon E5-2695v 2 CPU) with 256 GB of memory connected to BFS4 compute storage over a 1-GB network. Schrödinger’s Materials Science Suite Release 2014-3 (Ref. 29) was the primary software package used for the computations. Molecular structures for evaluation were constructed using *Maestro*, the visualization component of the Material Science Suite. *Maestro* includes a qualitative optimization routine that rapidly generates an approximate minimum-energy configuration of the molecular structure. Pre-optimized molecular structure files generated by *Maestro* were then used as input to the *Jaguar* computational chemistry engine contained in the Materials Science Suite for a more-rigorous geometry optimization using DFT. For certain molecular structures, it became necessary to repeat the DFT optimization process several times when the structures reached a level of complexity that exceeded the allowable iteration limits. The fully energy-minimized

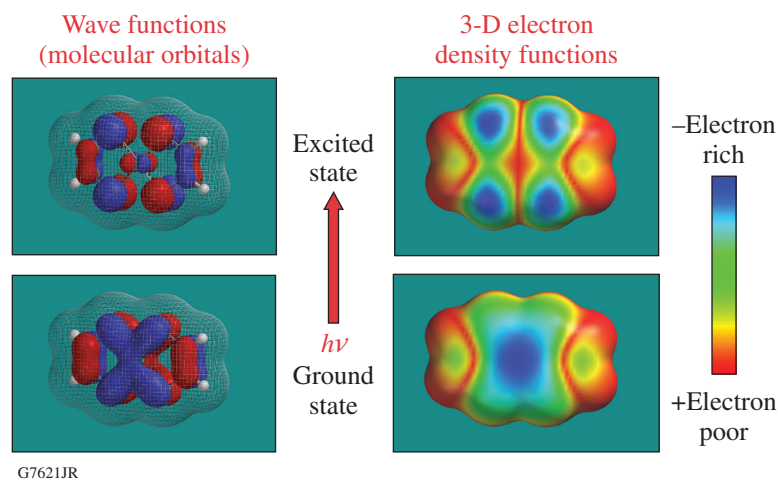


Figure 143.31

A comparison of computed visualizations of wave functions versus electron density functions for the same molecule.

structures were then used as input for the TDDFT calculations used to model the excited-state absorption spectra. (This work will be reported in a future publication.)

For ground-state geometry calculations, we used the basis set 6-31G** for the initial qualitative minimizations since it allowed us to use polarization on all atoms (including hydrogens); it can also produce good results with minimal computational resources. To determine single-point energy values for the *trans* and *cis* states of azobenzenes (and the corresponding open-ring and closed-ring forms of spiropyrans), we initially used the 6-311G-3DF-3PD basis set. This basis set has two sizes of extended Gaussian functions and produces a more-exact solution to the Schrödinger equation, but because of the large amount of computational resources required and long computation times (more than 168 h for one compound), it was used primarily for the final energy calculations.

Table 143.VI lists the computational parameters used to model all of the candidate materials evaluated in this study. Once this series of parameters had been established, only the

Table 143.VI: Computational parameters used to model the investigated candidate materials. The only variable for each computational run was the maximum number of iterations (shown in red), which needed to be increased for more-complex structures.

	Optimization	Energy
Input		
Basis Set	6-31G	6-311G-3DF-3PD
Polarization	**	none
Diffuse	none	none
Theory		
Level of theory	DFT	DFT
SCF spin treatment	restricted	restricted
Recommended	B3LYP	B3LYP
Self-consistent field		
Accuracy level	ultrafine	ultrafine
Initial guess	atomic overlap	atomic overlap
Maximum iterations	200	200
Energy change	5×10^{-5}	5×10^{-5}
rms density matrix change	5×10^{-6}	5×10^{-6}
Optimization		
Maximum steps	500	N/A
Convergence criteria	default	N/A
Initial Hessian	Schlegel guess	N/A
Output		
Calculation stage	At end of job	At end of job

iteration limits were changed to provide enough computing cycles for the self-consistent field (SCF) energy to converge for more-complex structures. Computation of the electronic spectrum for each compound after completing the DFT energy optimization is initiated by selecting the TDDFT option under the “Theory” tab of the *Jaguar* software menu.

Modeling Strategy

Our initial goal for this effort was to evaluate molecular structural elements that would contribute to a high level of bistability in the photoswitchable alignment layer. The following components are considered beneficial in achieving a high level of bistability for optical switching: (1) a significant difference in the isomerization activation energy; (2) a reduced potential energy level for the *cis* state to prevent relaxation back to the *trans* state; and (3) the free-space volume required by the core and pendants (for in-plane switching). The energy diagram in Fig. 143.32 shows how the first two parameters can affect system bistability. If the isomerization energy barrier between the two states becomes too large, it will become difficult to achieve optical switching.³⁰

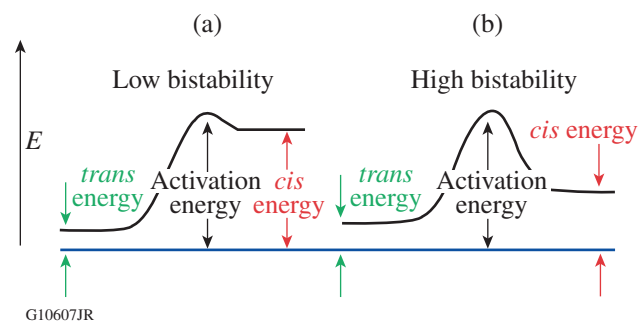


Figure 143.32

Comparison of energy diagrams for photoswitchable azobenzene alignment layers. (a) A system with low bistability. The activation energy barrier required to switch from the *trans* state to the *cis* state is large, while the energy barrier for the reverse transition from *cis* to *trans* is relatively shallow, making it easier to convert back to the *trans* isomer. (b) A system with high bistability. Here the energy barrier between both the *trans*–*cis* and *cis*–*trans* states is large, and once switched into the *cis* state, the material will remain in that state indefinitely. The large activation energy barrier also means that a larger amount of optical energy will be necessary to induce switching.

In this work, we concentrated on modeling the energy difference between the *trans* and *cis* states in methacrylate and acrylamide oligomers, which consist of a single photomechanically switchable chromophore substituted with various terminal functional groups that is linked by an alkyl spacer chain, or “tether,” to a backbone consisting of several methacrylate or acrylamide monomeric repeat units. Figure 143.33 shows a typi-

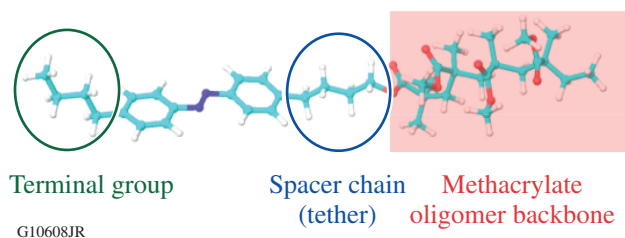


Figure 143.33

An example of a single azobenzene repeat unit used in the simulations. This azobenzene contains a four-carbon alkyl *terminal group* and is connected to the methacrylate oligomer on the far right by a four-carbon spacer chain, or *tether*. A large number of these short backbones consisting of such “repeat units” would be linked together to form the polymer backbone by polymerization of the methacrylate groups at the ends of the oligomer chain.

cal example of such a model compound based on a methacrylate backbone and an azobenzene chromophore.

Because of the large amounts of computational resources and time required to accurately model a complete polymer system with a large number of repeat units, we chose to limit the modeling to oligomers with only one tethered chromophore and four repeat units in the backbone. To compare the terminal functional group’s contributions to the *trans* and *cis* energy states, the alkyl spacer chain length was limited to four repeat units. Computational efforts focused on three different molecular aspects: (1) the length of the alkyl tether, (2) the composition of the terminal group attached to the azobenzene core, and (3) the oligomer backbone structure. Typical computation times for each oligomeric material ranged from 10 min to >96 h for geometry optimization and 5 min to >120 h for energy calculations, depending on the complexity of the structure.

Table 143.VII: Comparison of calculated versus literature values for a series of substituted azobenzene chromophores. Note that the calculated energy values in this table are expressed as negative numbers to aid comparison to literature values; elsewhere, energy differences are reported as the absolute values for simplicity.

	R ₁	R ₂	<i>trans</i> energy (hartrees)	<i>cis</i> energy (hartrees)	Energy difference (hartrees)	Energy difference (kJ/mol)	
						Calculated	Literature values ¹⁷
	H	H	-572.78	-572.75	0.0239	-62.69	-64.20
	OH	H	-648.00	-647.97	0.0250	-65.76	-69.50
	EtOH	H	-726.62	-726.60	0.0241	-63.26	-66.20
	NO ₂	NH ₂	-832.64	-832.62	0.0243	-63.39	-66.67
	H	NH ₂	-628.14	-628.11	0.0244	-64.19	-70.10

To initially test the modeling accuracy of the *Jaguar* software, we conducted *trans* and *cis* potential energy calculations using the 6-31G(d,p) basis set on a series of substituted azobenzene chromophores reported in the literature by Piyanzina *et al.*¹⁷ Table 143.VII compares the results obtained from these calculations to the literature values. The agreement between the calculated and literature results is remarkable, considering that Piyanzina *et al.* used in their calculations the more-complex (and computationally intensive) 6-31G++G (d,p) basis set that is reported to produce more-accurate results than 6-31G (d,p) because of the inclusion of additional functions that provide a better fit to the Schrödinger equation.

Results and Discussion

1. Azobenzene Chromophores

a. Effect of flexible alkyl tether length. The effect of alkyl tether length on the oligomer potential energy for materials containing an azobenzene core in the *trans* and *cis* isomeric states, respectively, was initially modeled with a methoxy group occupying the *para* position on the azobenzene core to reduce computation time. Methacrylate and acrylamide oligomers with backbones composed of four repeat units and alkyl tether chain lengths ranging from C₁ to C₁₂ were evaluated (Fig. 143.34). Table 143.VIII gives the calculated energies for the *trans* and *cis* states for the methacrylate and acrylamide oligomers, respectively. Both data sets are plotted in Fig. 143.35 for comparison.

For the methacrylates, alkyl tether lengths of 5, 6, 8, 9, and 11 carbon atoms produced lower differences in isomerization state energy, with the 6 and 11 carbon tethers providing the greatest reductions in the isomerization energy state. Sudden and steep variations in energy differences as the tether length increased

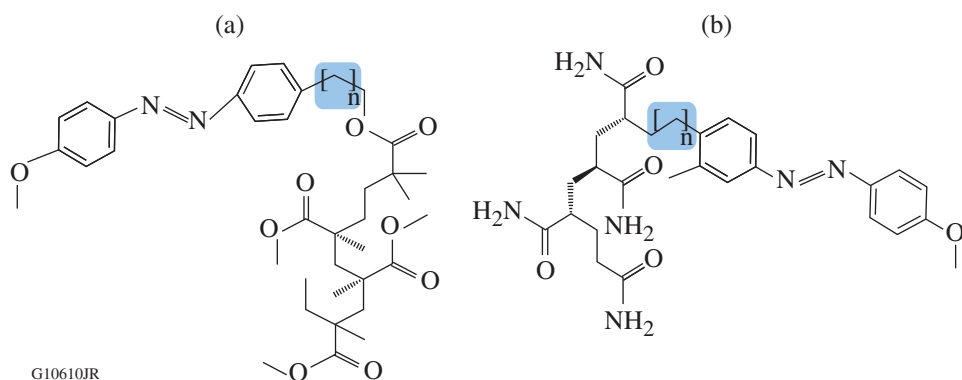


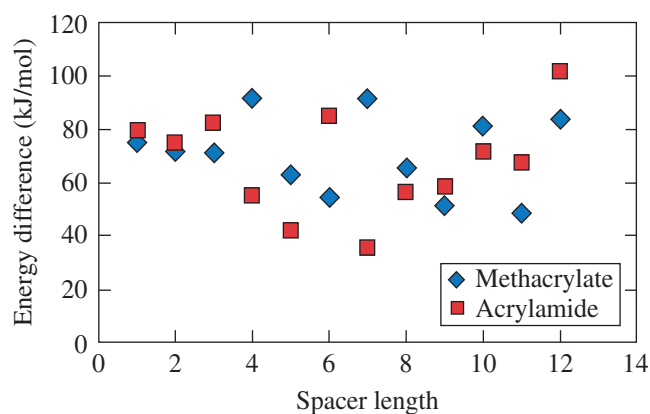
Figure 143.34

Molecular structures of the oligomeric methoxy-substituted azobenzene materials used to test the effect of alkyl tether length on potential energy in the *trans* and *cis* states: (a) methacrylate backbone; (b) acrylamide backbone. Both backbones were limited to four repeat units. The tether length n ranged from C_1 to C_{12} .

G10610JR

Table 143.VIII: Calculated potential energy difference values for the *trans* and *cis* energy states for methoxy-substituted azobenzene cores tethered to methacrylate and acrylamide backbones by alkyl chains ranging in length from 1 to 12 carbon atoms. The values in red indicate those materials with the lowest energy state differences.

Spacer length	<i>trans</i> energy (hartrees)	<i>cis</i> energy (hartrees)	Energy difference	
			(hartrees)	(kJ/mol)
Methacrylate backbone				
1	-2149.20	-2149.18	0.0285	74.87
2	-2188.53	-2188.50	0.0272	71.48
3	-2227.84	-2227.82	0.0271	71.22
4	-2267.16	-2267.13	0.0348	91.45
5	-2306.47	-2306.45	0.0241	63.20
6	-2345.78	-2345.76	0.0208	54.55
7	-2385.11	-2385.08	0.0350	91.90
8	-2424.40	-2424.38	0.0251	65.81
9	-2463.73	-2463.71	0.0195	51.15
10	-2503.06	-2503.03	0.0310	81.31
11	-2542.37	-2542.35	0.0184	48.36
12	-2581.69	-2581.66	0.0319	83.86
Acrylamide backbone				
1	-1715.97	-1715.94	0.0302	79.21
2	-1755.28	-1755.25	0.0286	75.16
3	-1794.59	-1794.56	0.0314	82.41
4	-1833.91	-1833.89	0.0210	55.18
5	-1873.23	-1873.21	0.0160	41.91
6	-1912.55	-1912.52	0.0323	84.88
7	-1951.86	-1951.84	0.0135	35.35
8	-1991.17	-1991.15	0.0215	56.32
9	-2030.49	-2030.47	0.0223	58.63
10	-2069.81	-2069.78	0.0271	71.27
11	-2109.12	-2109.10	0.0255	67.08
12	-2148.45	-2148.41	0.0387	101.64



G10611JR

Figure 143.35

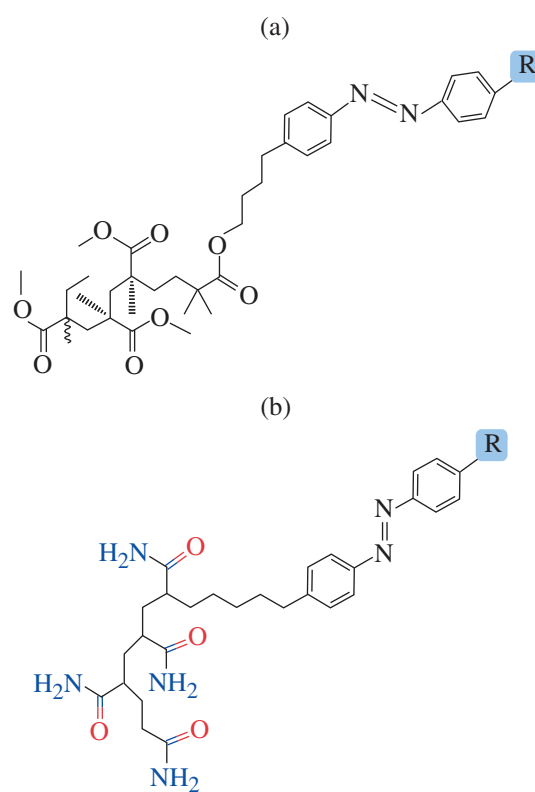
Plot of the calculated difference in energy between *trans* and *cis* states versus tether length for the data shown in Table 143.VIII.

were also observed, with an apparent odd–even effect occurring when the tether contained between 8 and 12 carbon atoms. We speculate that this effect may be caused by chain folding in the alkyl tether and must be investigated in more detail.

In contrast, the acrylamide oligomers show the lowest *trans*–*cis* isomerization energy differences when the alkyl tethers contains 4, 5, 7, 8, and 9 carbon atoms, with some of these values noticeably smaller than those of their methacrylate counterparts. No odd–even effect as a function of tether chain length is seen in this series. It would be of interest to see if the effect occurs if the tether length is longer than 12 carbon atoms. The large differences in isomerization state energies observed in the methacrylate oligomer with C_4 and C_7 tethers and the acrylamide oligomer with a C_{12} tether imply that these materials would be a poor choice for a photoalignment coating intended for bistable switching applications.

b. Effect of terminal groups. We evaluated 22 different terminal groups computationally to determine their individual effects on the potential energy difference between the *trans* and *cis* state when used as substituents on azobenzene cores linked through a four-carbon tether to the same methacrylate and acrylamide backbones used in the computations in the previous subsection. Representative structures for these oligomers are shown in Fig 143.36. Calculated values for both methacrylate and acrylamide oligomers with azobenzene cores are included as a benchmark reference.

Table 143.IX gives the calculated differences in the *trans* and *cis* energy states for oligomers containing alkyl-substituted



G10612JR

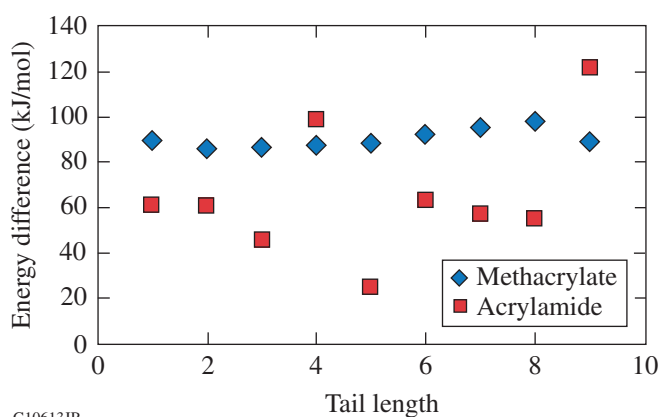
Figure 143.36

Molecular structures of the oligomeric azobenzene materials used to evaluate the effect of a variety of terminal groups (denoted as “R” in the figure) on potential energy in the *trans* and *cis* states: (a) methacrylate backbone; (b) acrylamide backbone. Both the backbones and alkyl tether chains were limited to four repeat units.

azobenzene chromophores. In Fig. 143.37, both data sets are plotted as a function of the terminal alkyl group carbon number for comparison. The alkyl terminal group length appears to have a limited ability to lower the isomerization state energy difference in the methacrylate oligomers. Only a slow, steady increase in energy difference between the *trans* and *cis* states is observed as the alkyl chain increases, reaching a maximum at C_8 and then dropping back at C_9 to the same value as seen for shorter chain lengths. In contrast, changing the alkyl terminal chain length in the acrylamide oligomers produces large fluctuations in isomerization state energy differences between C_3 and C_5 , a plateau between C_6 to C_8 , and a sharp jump at C_9 . All of the acrylamide oligomers (with the exception of those containing C_4 and C_9 terminal groups) show consistently lower *trans*–*cis* energy state differences than their methacrylate counterparts. They also show the lowest (25.10 for C_5) and highest (121.83 for C_9) energy differences of all evaluated alkyl terminal groups.

Table 143.IX: Calculated values of *trans-cis* isomerization energy for tethered azobenzenes with various alkyl terminal group lengths on methacrylate and acrylamide backbones. The azobenzene is tethered to the backbone using a four-carbon alkyl chain. The values in red indicate those materials with the lowest energy state differences.

Terminal group	<i>trans</i> energy (hartrees)	<i>cis</i> energy (hartrees)	Energy difference	
			(hartrees)	(kJ/mol)
Methacrylate backbone				
None	-2152.63	-2152.60	0.0333	87.50
Methyl	-2191.954	-2191.92	0.0342	89.78
Ethyl	-2231.27	-2231.24	0.0328	86.21
Propyl	-2270.59	-2270.55	0.0331	86.83
Butyl	-2309.90	-2309.87	0.0334	87.79
Pentyl	-2349.22	-2349.189	0.0336	88.24
Hexyl	-2388.54	-2388.50	0.0351	92.21
Heptyl	-2427.85	-2427.82	0.0366	96.02
Octyl	-2467.17	-2467.13	0.0373	97.85
Nonyl	-2506.49	-2506.45	0.0340	89.26
Acrylamide backbone				
None	-1719.40	-1719.37	0.0227	59.71
Methyl	-1758.71	-1758.68	0.0233	61.14
Ethyl	-1798.03	-1798.01	0.0232	60.90
Propyl	-1837.32	-1837.33	0.0175	45.82
Butyl	-1876.67	-1876.63	0.0377	98.97
Pentyl	-1915.97	-1915.96	0.0096	25.10
Hexyl	-1955.30	-1955.28	0.0243	63.67
Heptyl	-1994.60	-1994.58	0.0217	56.90
Octyl	-2033.92	-2033.90	0.0209	54.80
Nonyl	-2073.25	-2073.21	0.0464	121.83

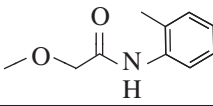
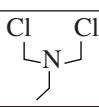
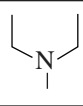


G10613JR

Figure 143.37
Plot of the difference in energy between *trans* and *cis* states versus alkyl terminal group length for the data shown in Table 143.IX.

Table 143.X lists the remaining terminal groups used as substituents on azobenzene methacrylate and acrylamide oligomers evaluated computationally for their *trans-cis* isomerization state energies. For the methacrylate oligomers shown in Table 143.X, the smallest difference in *trans-cis* isomerization energy levels occurs for those materials containing the cyanate ester and 2-methoxy-N-(2-methylphenyl) acetamide terminal groups. For these compounds, the *trans-cis* isomerization energy differences were lower than those for the same backbone containing an unsubstituted azobenzene core by 16% and 72%, respectively. The acrylamide oligomers also show a large decrease in *trans-cis* isomerization state energy differences with the 2-methoxy-N-(2-methylphenyl) acetamide group (62%). The fluoroalkane terminal group produced the largest decrease in the study (nearly 70% lower than the unsubstituted azobenzene core).

Table X: Calculated values of *trans*–*cis* isomerization energy for tethered azobenzenes with a variety of terminal groups on methacrylate and acrylamide backbones.

Backbone	Terminal group	Structure	<i>trans</i> energy (hartrees)	<i>cis</i> energy (hartrees)	Energy difference (hartrees)	Energy difference (kJ/mol)
Methacrylate	None		-2152.63	-2152.60	0.0333	87.50
Acrylamide			-1719.40	-1719.37	0.0227	59.71
Methacrylate	Chloro	— Cl	-2612.23	-2612.19	0.0338	88.71
Acrylamide			-2179.00	-2178.97	0.0229	60.06
Methacrylate	Fluoro	– F	-2251.87	-2251.83	0.0336	88.11
Acrylamide			-1818.62	-1818.61	0.00676	17.76
Methacrylate	Trichloromethyl	– CCl ₃	-3570.71	-3570.68	0.0322	84.62
Acrylamide			-3137.45	-3137.43	0.0214	56.09
Methacrylate	Trifluoromethyl	– CF ₃	-2489.67	-2489.64	0.0303	79.58
Acrylamide			-2056.43	-2056.41	0.0247	64.73
Methacrylate	Cyanate ester	—O—C≡N	-2320.06	-2320.03	0.0278	73.07
Acrylamide			-1886.80	-1886.70	0.0274	71.99
Methacrylate	Hydroxyl	— OH	-2227.86	-2227.82	0.0336	88.17
Acrylamide			-1794.61	-1794.58	0.0321	84.35
Methacrylate	2-methoxy-N-(2-methylphenyl)acetamide		-2706.24	-2706.23	0.00939	24.65
Acrylamide			-2272.94	-2272.93	0.00855	22.46
Methacrylate	Amino	— NH ₂	-2207.99	-2207.96	0.0336	88.25
Acrylamide			-1774.72	-1774.70	0.0219	57.47
Methacrylate	Nitrile	C≡N	-2244.88	-2244.84	0.03304	86.76
Acrylamide			-1811.58	-1811.60	0.0208	54.50
Methacrylate	N, N-bis (chloromethyl)ethanamine		-3245.11	-3245.08	0.0305	80.02
Acrylamide			-2811.81	-2811.79	0.0261	68.54
Methacrylate	Diethylamino		-2365.24	-2365.21	0.0305	79.98
Acrylamide			-1932.00	-1931.97	0.0236	62.07
Methacrylate	Piperidine		-2403.36	-2403.32	0.034	90.70
Acrylamide			-1970.12	-1970.09526	0.0280	73.45
Methacrylate	Pyrrolidine		-2364.00	-2364.001	0.03340	89.25
Acrylamide			-1930.81	-1930.78	0.0235	61.79

G10625JR

2. Spiropyran Chromophores

Preliminary modeling using the same methods as used for **Azobenzene Chromophores** (p. 154) was applied to acrylamide oligomers containing methoxy-substituted spiropyran chromophores tethered to the backbone using alkyl chains of varying lengths [Fig. 143.38(a)]. Unlike azobenzenes, where no bonds are broken during photoisomerization, spiropyrans

undergo a reversible photomediated ring opening/closing reaction upon absorption of UV and visible light [Fig. 143.38(b)].

Table 143.XI compares the calculated energy difference between the closed and open forms for an unsubstituted spiropyran chromophore tethered to an acrylamide oligomer backbone by a C₄ alkyl chain to the calculated *trans*–*cis* photo-

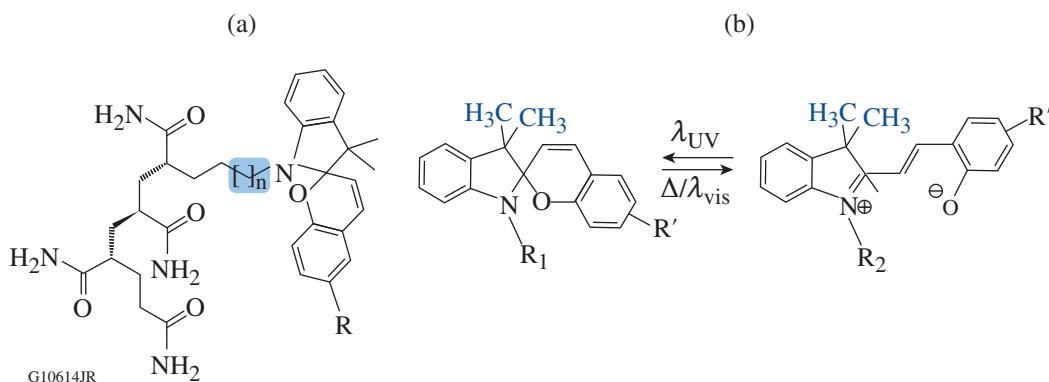


Figure 143.38

(a) A methoxy-substituted spiropyran tethered with alkyl chains of differing lengths to an acrylamide backbone (the tether is shaded in blue); (b) the mechanism for photomediated ring opening/closing reaction in spiropyrans.

Table 143.XI: The calculated energy difference between the closed and open forms for an unsubstituted spiropyran chromophore tethered to an acrylamide backbone by a C₄ alkyl chain. For comparison we have included the calculated energy differences for the *trans*–*cis* photoisomerization states in an unsubstituted azobenzene chromophore connected to an acrylamide backbone or methacrylate backbone using the same tether length.

Backbone	Chromophore	Terminal group	Spacer length	Open-form energy (hartrees)	Closed-form energy (hartrees)	Energy difference	
						(hartrees)	(kJ/mol)
Acrylamide	Azobenzene	None	4	-1719.40	-1719.37	0.0227	59.71
	Spiropyran			-1972.72	-1972.75	0.0316	83.01
Methacrylate	Azobenzene			-2152.63	-2152.60	0.0333	87.50

isomerization energy differences for unsubstituted azobenzene chromophores connected to acrylamide and methacrylate backbones using the same tether length. Although the energy state differences for the spiropyran acrylamide oligomer are higher than for the corresponding azobenzene oligomer, they are comparable to those calculated for the azobenzene chromophore connected to a *methacrylate* backbone through a C₄ alkyl chain. Calculations are in progress to determine the closed-form and open-form energy differences for other spiropyran oligomers with methacrylate, acrylamide, and siloxane backbones tethered to substituted spiropyran chromophores using a variety of alkyl chain lengths.

Conclusions and Future Work

Computational modeling was used to determine the properties of a series of oligomeric methacrylate and acrylamide photoswitchable alignment layer materials intended as potential candidates for use in an optically switchable LC laser beam shaper. Photoisomerization energy state differences in model compounds were calculated using DFT and TDDFT compu-

tational methods (Materials Science Suite, Schrödinger, Inc.) employing the 6-31G** basis set. Twenty-two different terminal functional groups were evaluated computationally to determine their individual effects on the energy difference between the *trans* and *cis* isomerization-state energy levels (one of the three factors affecting bistability in photoswitchable alignment layers) when they were used as substituents on azobenzene cores linked through a four-carbon tether to methacrylate and acrylamide backbones. The effect of the alkyl tether connecting the chromophore to the oligomer backbone on the isomerization state energy differences of the methacrylate and acrylamide oligomers was also investigated computationally. This work revealed a number of key findings:

1. When methoxy-substituted azobenzene chromophores are tethered to a *methacrylate oligomer*, lower energy differences between the *trans* and *cis* isomerization states occur for alkyl tether lengths of 5, 6, 8, 9, and 11 carbons. The C₆ and C₁₁ tethers produce the smallest energy difference, implying that they are a good choice for a photoalignment

coating intended for bistable switching applications. For the same core and an alkyl tether length of C₄, replacing the methoxy terminal group on the azobenzene core with alkyl groups up to C₉ appears to have a limited ability to lower the isomerization-state energy difference, while cyanate ester and 2-methoxy-N-(2-methylphenyl) acetamide terminal groups are highly effective in producing the smallest differences in *trans*–*cis* isomerization energy levels.

2. *Acrylamide oligomers* tethered to a methoxy-substituted azobenzene chromophore show the smallest *trans*–*cis* isomerization energy differences for alkyl tethers containing 4, 5, 7, 8, and 9 carbon atoms, in some cases considerably smaller than those of the corresponding methacrylate oligomers. Unlike what was seen for methacrylate oligomers, replacing the methoxy group on the azobenzene core with C₅ and C₉ terminal alkyl groups shows a *significant* reduction in *trans*–*cis* isomerization-state energies. With the exception of C₄ and C₉ terminal groups, all of the acrylamide oligomers with alkyl-substituted azobenzene cores show consistently lower *trans*–*cis* isomerization-state energy differences than do their methacrylate counterparts. Other terminal functional groups that show a large decrease in *trans*–*cis* isomerization-state energy differences are the 2-methoxy-N-(2-methylphenyl) acetamide group (62%) and the fluoroalkane terminal group (70%) as compared to an unsubstituted azobenzene core.
3. With only a few exceptions, acrylamide oligomers as a group exhibit lower *trans*–*cis* isomerization energy differences than methacrylate oligomers with the same structure, making them (in the absence of other factors) preferred candidates for photoswitchable device applications where good bistability is required.

Considerable work remains in developing these computational tools and methodologies into a reliable, predictive capability for photoswitchable alignment layer design. The observed odd–even effect in the *trans*–*cis* isomerization energies as a function of tether chain length seen for methoxy-azobenzene-methacrylate oligomer systems must be more fully investigated for longer tether lengths and on different oligomeric backbones (e.g., methacrylate, acrylamide, siloxane) to determine if it is specific to one oligomer class. Both the transition state energy and the swept volume produced by motion of the chromophore pendant (both azobenzenes and spiropyranes) will be determined by transition state modeling (DFT) and molecular dynamics simulations using the *Jaguar* and *Desmond* components of the Materials Science Suite,

respectively. Highly intensive computational modeling of systems with up to 15 or more backbone segments, along with targeted synthesis and characterization of the most-promising candidate materials from these studies, will lead to both a more-detailed understanding of these materials systems and sufficient quantities of materials for characterization studies and device development activities.

ACKNOWLEDGMENT

This material is based upon work supported by the Department of Energy National Nuclear Security Administration under Award Number DE-NA0001944, the University of Rochester, and the New York State Energy Research and Development Authority. The support of DOE does not constitute an endorsement by DOE of the views expressed in this article. The authors acknowledge M. Charissis of LLE's Computer Support Group for his help in supporting our computation efforts on LLE's Computing Facility. We also acknowledge Dr. S. Kwak and Dr. S. Murdock of Schrödinger LLC for their helpful discussions and guidance in conducting this work.

REFERENCES

1. C. Dorrer, S. K. H. Wei, P. Leung, M. Vargas, K. Wegman, J. Boulé, Z. Zhao, K. L. Marshall, and S. H. Chen, *Opt. Lett.* **36**, 4035 (2011).
2. K. L. Marshall, S. K.-H. Wei, M. Vargas, K. Wegman, C. Dorrer, P. Leung, J. Boule III, Z. Zhao, and S. H. Chen, in *Liquid Crystals XV*, edited by I. C. Khoo (SPIE, Bellingham, WA, 2011), Vol. 8114, Paper 81140P.
3. K. L. Marshall, C. Dorrer, M. Vargas, A. Gnolek, M. Statt, and S.-H. Chen, in *Liquid Crystals XVI*, edited by I. C. Khoo (SPIE, Bellingham, WA, 2012), Vol. 8475, Paper 84750U.
4. K. L. Marshall, J. Gan, G. Mitchell, S. Papernov, A. L. Rigatti, A. W. Schmid, and S. D. Jacobs, in *Liquid Crystals XII*, edited by I. C. Khoo (SPIE, Bellingham, WA, 2008), Vol. 7050, Paper 70500L.
5. S. R. Nersisyan *et al.*, *Opt. Express* **21**, 8205 (2013).
6. K. L. Marshall, D. Saulnier, H. Xianyu, S. Serak, and N. Tabiryan, in *Liquid Crystals XVII*, edited by I. C. Khoo (SPIE, Bellingham, WA, 2013), Vol. 8828, Paper 88280N.
7. J. Vernon *et al.*, *Crystals* **3**, 234 (2013).
8. J. P. Vernon *et al.*, *Opt. Express* **21**, 1645 (2013).
9. J. P. Vernon *et al.*, *Advanced Optical Materials* **1**, 84 (2013).
10. M. Schadt, H. Seiberle, and A. Schuster, *Nature* **381**, 212 (1996).
11. K. Ichimura, *Chem. Rev.* **100**, 1847 (2000).
12. A. Muravsky *et al.*, *J. Soc. Inf. Disp.* **15**, 267 (2007).
13. O. Yaroshchuk and Y. Reznikov, *J. Mater. Chem.* **22**, 286 (2012).
14. K. L. Marshall, O. Didovets, and D. Saulnier, in *Liquid Crystals XVIII*, edited by I. C. Khoo (SPIE, Bellingham, WA, 2014), Vol. 9182, Paper 91820J.

15. E. G. Lewars, *Computational Chemistry: Introduction to the Theory and Applications of Molecular and Quantum Mechanics*, 2nd ed. (Springer, Dordrecht, The Netherlands, 2011).
16. P. C. Chen and Y. C. Chieh, *J. Mol. Struct. (Theochem)* **624**, 191 (2003).
17. I. Piyanzina *et al.*, *J. Mol. Model.* **21**, 1 (2015).
18. C. Ruslim and K. Ichimura, *Macromolecules* **32**, 4254 (1999).
19. M. C. Zerner, *ZINDO, A Semiempirical Quantum Chemistry Program*, Quantum Theory Project (University of Florida, Gainesville, FL, 1996).
20. W. J. Hehre, *Ab Initio Molecular Orbital Theory* (Wiley, New York, 1986).
21. I. N. Levine, *Quantum Chemistry*, 4th ed. (Prentice-Hall, Englewood Cliffs, NJ, 1991), pp. 455–544.
22. C. J. Cramer, *Essentials of Computational Chemistry: Theories and Models* (J. Wiley, West Sussex, England, 2002), pp. 153–189.
23. E. Runge and E. K. U. Gross, *Phys. Rev. Lett.* **52**, 997 (1984).
24. K. I. Ramachandran, G. Deepa, and K. Namboori, *Computational Chemistry and Molecular Modeling: Principles and Applications* (Springer-Verlag, Berlin, 2008).
25. D. Jacquemin *et al.*, *J. Chem. Phys.* **124**, 74104 (2006).
26. D. Jacquemin *et al.*, *J. Chem. Phys.* **121**, 1736 (2004); M. Dubecký *et al.*, *J. Chem. Phys.* **133**, 244301 (2010).
27. E. A. Perpète *et al.*, *J. Chem. Theory Comput.* **2**, 434 (2006).
28. K. L. Marshall, R. Wang, M. Coan, A. G. Noto, K. Leskow, R. Pauszek, and A. Moore, in *Liquid Crystals XI*, edited by I. C. Khoo (SPIE, Bellingham, WA, 2007), Vol. 6654, Paper 66540F.
29. Schrödinger Materials Science Suite, Release 2014-3 (Jaguar, ver. 8.5 and Maestro, ver. 9.9), Schrödinger, New York, NY 10036-4041.
30. J. G. Meier, R. Ruhmann, and J. Stumpe, *Macromolecules* **33**, 843 (2000).